

LEARNING VECTOR QUANTIZATION FOR COLOR CLASSIFICATION OF DISEASED AIR SACS IN CHICKEN CARCASSES

J. G. Ibarra, Y. Tao, L. Newberry, Y. R. Chen

ABSTRACT. *The variation in color features observed during the evolution of air-sacculitis in chicken carcasses is exploited to classify the disease using digital imaging and neural networks. For the experiments, air-sacculitis was induced by secondary infected of E. coli via direct inoculation of challenge bacteria. Mild and severely infected samples were obtained and imaged. For the supervised classification, a knowledge base set of normalized RGB values, corresponding to negative, mild, and severely infected air sac images, was obtained. Statistical data exploration indicated no significant difference between the color features of mild and severely infected sacs, but a significant difference was found between infected and negative tissues. A neural network using the learning vector quantization algorithm classified the data in infected and negative categories. Resubstitution and hold-out errors were calculated, giving an overall accuracy in the classification of 96.7%. Each poultry carcass sold in the U.S. must be visually inspected for its wholesomeness by a USDA inspector, with air-sacculitis being the major cause of condemnation in poultry processing plants. The method presented here has the potential for integration in a computer-assisted inspection of wholesomeness in poultry processing lines.*

Keywords. *Air-sacculitis, Imaging, Neural networks, Color classification, Poultry disease inspection, Food safety.*

Since 1959, each poultry carcass sold in the U.S. has been visually inspected for wholesomeness at a poultry processing plant by USDA personnel. Because of the increasing demand for poultry products by consumers, the speed of the inspection process has been increased from 30 to 90 birds per min. The Food Safety and Inspection Service (FSIS) in the U.S. recognized that “the failure to apply sufficiently modern techniques to detect abnormalities in organs and tissues necessitates more extensive, yet less efficient, human resources during inspection.” The FSIS also recognized that computer imaging would greatly improve the inspection procedures (USDA-FSIS, 1985).

Much work has been devoted to the automatic inspection of wholesomeness in chicken carcasses. Most of the research is based on different optical techniques, mainly spectroscopy. Chen (1992), Chen and Massie (1993), and Chen et al. (1996) used visible/near-infrared (NIR) spectroscopy for the classification of wholesome, septicemic, and cadaver carcasses.

Those studies were conducted using an NIR probe with its housing about 2 cm from the skin of the carcass. Chen and Hruschka (1998) made on-line trials of a system for chicken carcass external inspection based on visible/NIR reflectance. The system was able to successfully identify 95% of the carcasses at a speed of 70 birds per min. Fiber optic spectroscopy was also used for the classification of diseases in slaughtered poultry (Park et al., 1998). Park et al. (1996) proposed the combination of multi-spectral imaging and neural network analyses. In that research, two cameras with filters at 540 nm and 700 nm and a backpropagation algorithm were used for the inspection of wholesomeness in poultry carcasses.

As for the detection of lesions commonly observed in the body cavity, Chao et al. (1998) analyzed the size and coloration of liver in infected poultry. In related research (Tao et al., 1998a, 1998b, 2000), the size and color features of infected enlarged spleen in turkeys were studied. Both studies were performed in laboratory conditions, with the viscera prepared prior to the experimentation.

Color processing is also very popular in agriculture. Précetti and Krutz (1993) presented a detailed study of color classification algorithms and the potential for agricultural applications. Chtioui et al. (1998) used probabilistic neural networks for food classification. Specifically, they graded french fries in three categories according to color coordinates in the hue-saturation-intensity space.

In this work, a method for the classification of air-sacculitis lesions in chicken carcasses induced by secondary infection with *Escherichia coli* (*E. coli*) is proposed. The specific objectives of this work were:

- To establish a procedure for controlled induction of air-sacculitis.

Article was submitted for review in Nov. 2000; approved for publication by the Information & Electrical Technologies Division of ASAE in June 2002.

The authors are: **Juan G. Ibarra, ASAE Member**, Photonics and Sensors Group Leader, John V. Newman Research Center, Sunkist Growers, Inc., Ontario, California; **Yang Tao, ASAE Member Engineer**, Associate Professor, Department of Biological Resources Engineering, University of Maryland, College Park, Maryland; **Lisa Newberry**, Research Associate, Poultry Science, University of Arkansas, Fayetteville, Arkansas; and **Yud-Ren Chen, ASAE Member Engineer**, Research Leader, Instrumentation and Sensing Lab. USDA Agricultural Research Service, Beltsville Maryland. **Corresponding author:** Dr. Yang Tao, Biological Resources Engineering, University of Maryland, College Park, MD 20742; phone: 301-405-1189; fax: 301-314-9023; e-mail: ytao@wam.umd.edu.

- To establish red–green–blue (RGB) transformation for optimal classification.
- To implement neural network classification of air sacs color features based on the learning vector quantization (LVQ) technique.

Each poultry carcass sold in the U.S. must be visually inspected for its wholesomeness by an USDA inspector, with air–sacculitis being the major cause of condemnation in poultry processing plants. The method presented here has the potential for integration in a computer–assisted inspection of wholesomeness in poultry processing lines.

MATERIALS AND METHODS

AIR–SACculITIS INDUCTION

Besides the diseases present in the exterior of poultry carcasses (septicemia, cadaver, bruise, and tumor), a bird can be rejected from the production line due to diseases observed in the internal cavity. Spleen enlargement, air–sacculitis, and liver coloration are common indicators of internal diseases, with air sacs infection being the major cause of condemnation in a poultry processing plant, especially during winter (Herenda and Franco, 1996). The air sac system in a chicken consists of eight membranous air bags that are part of the respiratory system and are present to give the bird buoyancy in flight. Inspired air is taken in through the nares, trachea, bronchia, and lungs and expired into the air sacs. The mucociliary apparatus that is present in the sinuses, trachea, and bronchia cleans the inspired air.

Viruses, bacteria, and environmental factors (ammonia) can damage the mucociliary apparatus, allowing the entrance of bacteria that are normally swept out of the respiratory system by action of cilia and mucus, which entrap the bacteria and move them back up and out of the respiratory system. If bacteria, especially *E. coli*, pass this primary defense mechanism, then they can easily infect the air sacs, causing an influx of inflammatory cells. Along with the infection, the reaction causes the production of an exudate that can be localized or become generalized in the body cavity of the bird (Herenda and Franco, 1996). This inflammatory reaction can be mild to severe. If the condition is severe, then there is consolidation of the exudate in and around various organs. In practice, the evolution of the disease can be detected by the change in appearance and color of air sacs, from a transparent, thin, and smooth membrane in a healthy bird to an opaque, yellow, and rough tissue for severe infection.

To induce air–sacculitis in different degrees, a lactose–negative pathogenic strain of *E. coli*, isolated from a turkey with severe colibacillosis, was used as the challenge bacteria (see Huff et al., 1998, for details). The stock bacteria was grown overnight on blood agar and afterwards was inoculated into tryptose phosphate broth. The bacteria were then grown in a shaking water bath for 2.5 h at 37°C to the logarithmic phase of growth. At the end of the incubation, the bacteria was titrated and then stored at 4°C. Preliminary tests were conducted using the procedure described above. Chickens were inoculated with 0.2 mL into the posterior thoracic air sac using a tuberculin syringe and a 26–gauge needle. Two doses of bacteria were used for the experiments: 10³ and 10⁶ cells/mL. The doses with higher concentration

produced the best lesions (mostly severe cases), but the mortality was 2 out of 5 birds inoculated.

IMAGING SYSTEM

An imaging system was designed and built to capture images of the chicken carcass cavities under controlled conditions. The system is depicted in figure 1. For image acquisition, a Sony XC711 (Sony Component Products Co., Cypress, Cal.) CCD camera with RGB channels was connected to a Matrox Meteor II (Matrox Electronic Systems Ltd, Durval, Canada) image grabber. A Pentium computer hosted the image grabber. The CCD camera was previously calibrated for optimal color signal. For proper air sac visualization, the CCD camera was equipped with a Tokina 1:1.8/12.5–75 mm zoom lens (THK Photoproducts, Inc., Long Beach, Cal.) with a 2 mm extension tube to improve close focusing capability. A photographic stand held the camera and lens in vertical position, and eight “cool white” 18–inch fluorescent tubes (General Electric Lighting, Winchester, Va.) attached to semi–circular frames ensured uniform illumination of chicken cavities. The chicken carcasses were positioned at the base of the photographic stand in such a manner that the entire cavity could be imaged. The imaging system was installed in a closed aluminum chamber to avoid any ambient interference.

SAMPLES AND EXPERIMENTAL PROCEDURE

A total of 100 chickens were processed and imaged in these experiments. The chickens used were 6 weeks old and

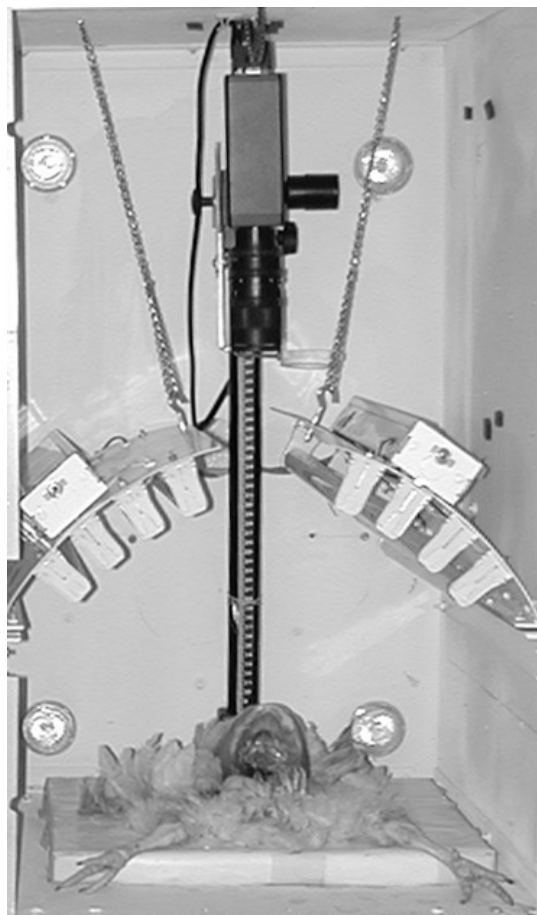


Figure 1. Experimental setups for air–sacculitis imaging.

obtained from a poultry processor. The birds were separated in two 50-sample batches, which were placed in separate floor pens and processed on two consecutive days. After inoculation, they were kept in the floor pen facility for three days to allow the infection to spread in the air sacs. After the waiting period, the birds were slaughtered and carefully bled to reduce the presence of blood or blood clots in the cavity images. Each sample was then opened through the abdomen and eviscerated, taking care to preserve the air sacs. Lesions similar in appearance and extension were obtained in both batches. Because bacteria were inoculated in a thoracic air sac, the disease was very well localized in one side of the cavity, while the other side remained without infection in most of the cases. This provided a convenient way to compare a negative with an infected sac in the same image.

The distribution of samples in each batch was 30 birds inoculated for severe infection, 15 for mild infection, and 5 not inoculated for control. Eight birds from the first batch and 14 from the second batch died before the imaging process. The dead birds were excluded from the experiment. To ensure proper classification, the birds were reclassified during the slaughtering into negative, mild, and severely infected, according to a visual inspection of the air sacs.

The images were grabbed and saved in the computer using a program written in Microsoft Visual Basic 5.0 (Microsoft Corp., Redmond, Wash.) The program utilized the Matrox Active MIL 5.11 (Matrox Electronics Systems Ltd., Quebec, Canada) library to interface with the frame grabber and automatically record images and information about the degree of lesion. The images consisted of three layers of 640×480 pixels (one for each color component) with pixel values between 0 and 255. Image analysis was performed using Matlab Image Processing Toolkit (Mathworks, Inc., Natick, Mass.) and a customized Graphic User Interface. Knowledge base color points were obtained by manually selecting in each image 30×30 pixel regions of interest (ROI) of severe, mild, and negative air sacs. Then, the pixel values in the ROI were transformed to the range 0 to 1 by dividing the corresponding value by 255. After that, the transformed RGB values at the location (x,y) inside the ROI were normalized according to (Gonzalez and Wood, 1992):

$$r(x,y) = \frac{R(x,y)}{R(x,y) + G(x,y) + B(x,y)} \quad (1a)$$

$$g(x,y) = \frac{G(x,y)}{R(x,y) + G(x,y) + B(x,y)} \quad (1b)$$

$$b(x,y) = \frac{B(x,y)}{R(x,y) + G(x,y) + B(x,y)} \quad (1c)$$

The representative rgb components for each ROI were taken as the average values of normalized color components in equations 1a, 1b, and 1c. It must be pointed out that the normalized color components in equation 1 remove the intensity variance from the RGB images (Jain and Kasturi, 1995). Moreover, it is easy to see that the normalized color components fulfill the condition $r + g + b = 1$.

Approximately four ROIs were selected and processed for each image. Each processed ROI was visually classified as negative, mild, or severe, and that lesion information along with the corresponding average normalized RGB values

(denoted hereafter as rgb) formed the knowledge base set for the classification. A total of 322 knowledge base points were obtained in this manner. The final distribution of lesions in the knowledge base set was 68 mild, 150 negative, and 104 severe. Figure 2 shows the distribution in the rgb space. The plane $r + g + b = 1$, which has intersections at $(1,0,0)$, $(0,1,0)$, and $(0,0,1)$ in the rgb space, is denoted here as plane [111] using the crystallographic notation (fig. 2). All the knowledge base points lay in that plane.

STATISTICAL ANALYSIS OF LESION GROUPS

Visualization of knowledge base points in figure 2 reveals an apparent separation between negative points and mild and severe points, but it appears that mild and severe points are not separated in the rgb space. A statistical analysis was used to compare means.

An ANOVA on the rgb data was performed to determine if a significant difference exists between the mean of the infection classes. The analysis indicates what was expected from the visual inspection of the data: There was a significant difference, at the 95% confidence level, between negative color component points and mild and severe color component points, and no significant difference, at the 95% confidence level, was observed between mild and severe color component points. As a consequence, the knowledge base set was modified to consider only negative and infected (mild + severe) observations.

This reclassification of the knowledge base set does not affect the potential application of the method, because the final assessment of carcass wholesomeness is given by an estimation of the extension of air sac exudate, instead of the evaluation of the degree of infection (Ewing, 1997).

It is worth noting that the apparent separation of knowledge base points in the plane [111] makes the color transformation simpler. For instance, a conventional HSI transform will introduce extra computations.

COLOR TRANSFORMATION AND CLASSIFICATION ALGORITHM

REDUCTION TO INDEPENDENT COLOR COMPONENTS

The normalization condition $r + g + b = 1$ allows reducing the number of color components to only two. This can be accomplished by transforming the rgb coordinate system to a new one with the origin in the center of gravity of the triangular plane [111] (located at $r = g = b = 1/3$) and with the new b-axis normal to the [111] plane. The transformation is illustrated in figure 3. The rotation can be described with the Euler angles θ , ϕ , and ψ , also referred as pitch, yaw, and roll, respectively (Goldstein, 1980). In this case, taking positive angles in a clockwise direction, the Euler angles for the transformation are:

$$\theta = 54.74^\circ \quad (2a)$$

$$\phi = 45^\circ \quad (2b)$$

$$\psi = -45^\circ \quad (2c)$$

The transformation matrix is then expressed as:

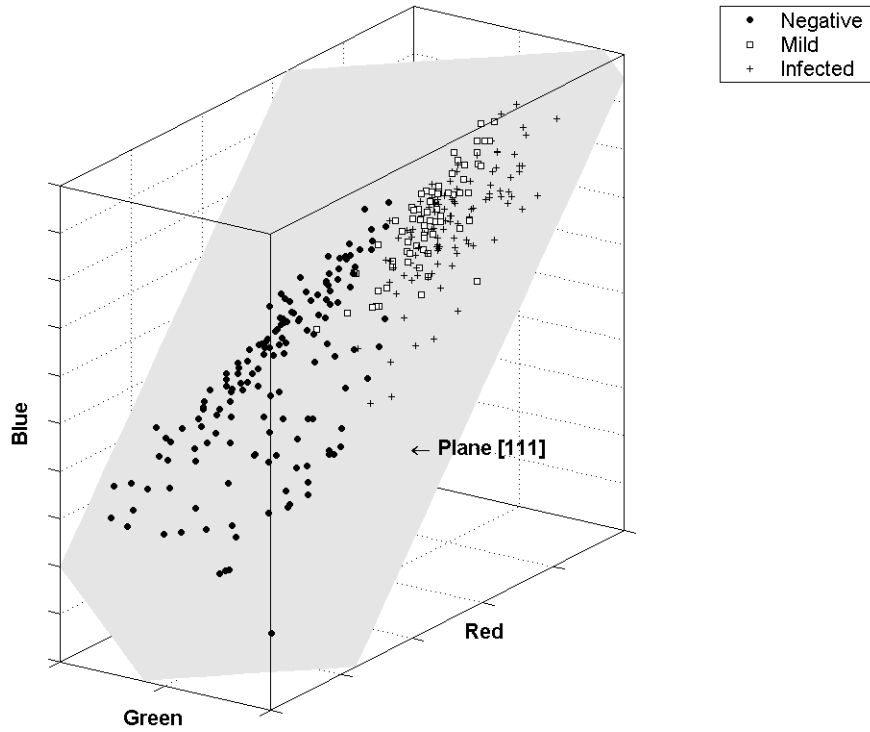


Figure 2. Knowledge base set in rgb space according to lesions. Circles indicate negative infection, squares mild infection, and plus signs severe infection. A fraction of the plane $r + g + b = 1$ (plane [111]) is also illustrated. All points lie in plane [111]. No apparent differences exist between mild and severe points.

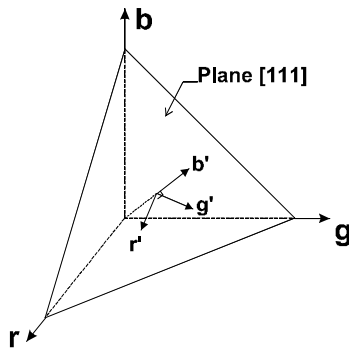


Figure 3. Axis transformation for reduction of color components. The new color frame $r'g'b'$ lies in plane [111], with axis b' normal to that plane.

$$\mathbf{A} = \begin{pmatrix} \frac{1}{2}\left(\frac{1}{\sqrt{3}}+1\right) & \frac{1}{2}\left(\frac{1}{\sqrt{3}}-1\right) & -\frac{1}{\sqrt{3}} \\ \frac{1}{2}\left(\frac{1}{\sqrt{3}}-1\right) & \frac{1}{2}\left(\frac{1}{\sqrt{3}}+1\right) & -\frac{1}{\sqrt{3}} \\ \frac{1}{\sqrt{3}} & \frac{1}{\sqrt{3}} & \frac{1}{\sqrt{3}} \end{pmatrix} \quad (3)$$

Applying the translation to the center of gravity of plane [111], the transformation equation for the new color components, say $r'g'b'$, is:

$$\begin{bmatrix} r' \\ g' \\ b' \end{bmatrix} = \mathbf{A} \begin{bmatrix} r-1/3 \\ g-1/3 \\ b-1/3 \end{bmatrix} \quad (4)$$

From equations 3 and 4, the final transformation of color components is:

$$r' = \frac{r}{2}\left(\frac{1}{\sqrt{3}}+1\right) + \frac{g}{2}\left(\frac{1}{\sqrt{3}}-1\right) - \frac{b}{\sqrt{3}} \quad (5a)$$

$$g' = \frac{r}{2}\left(\frac{1}{\sqrt{3}}-1\right) + \frac{g}{2}\left(\frac{1}{\sqrt{3}}+1\right) - \frac{b}{\sqrt{3}} \quad (5b)$$

while the new color component b' is zero. Note that the new color components r' and g' are independent.

The transformed color components r' and g' in equation 5 along with the lesion category (infected and negative) form the final knowledge base set for the supervised neural network, which is analyzed next.

LEARNING VECTOR QUANTIZATION

Learning vector quantization (LVQ) is a method for training competitive networks in a supervised manner. It presents more flexibility than a perceptron network and more robustness than a backpropagation algorithm (Hagan et al., 1996). The architecture of the LVQ network is shown in figure 4. The input is the vector \vec{p} formed by Q transformed color components r' and g' . The final output (\vec{i}) is the lesion category, which was defined as:

$$\vec{i} = \begin{cases} \begin{bmatrix} 1 \\ 0 \\ 0 \end{bmatrix} & \text{if negative} \\ \begin{bmatrix} 0 \\ 0 \\ 1 \end{bmatrix} & \text{if infected.} \end{cases} \quad (6)$$

The network consists of two layers. The first layer, or competitive layer, groups the inputs with similar color components according to relative distances. A linear layer completes the LVQ network. This second layer classifies the grouped color component inputs according to lesion category. The algorithm and learning process can be illustrated by

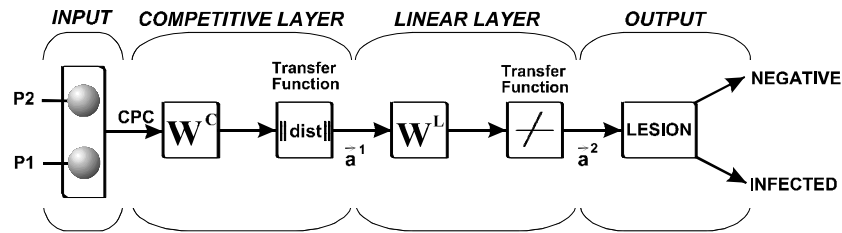


Figure 4. LVQ neural network architecture for color coordinates classification in infected and negative categories.

following the first iteration in the network. Let us indicate the input vectors from the knowledge base set as $\{\vec{p}_1, \vec{p}_2, \dots, \vec{p}_Q\}$ and the corresponding lesion category as $\{\vec{t}_1, \vec{t}_2, \dots, \vec{t}_Q\}$. To start, the row vectors in the competitive weight matrix (\mathbf{W}^C) are set to random values. On the other hand, the linear weight matrix (\mathbf{W}^L) only groups the input vectors into two categories (with no subcategories). The explicit form of this matrix is:

$$\mathbf{W}^L = \begin{bmatrix} 1 & 0 \\ 0 & 1 \end{bmatrix} \quad (7)$$

When the first input vector is presented, the first layer calculates the distance between it and the vectors in \mathbf{W}^C with the condition that the closest vector in the weight matrix wins the competition. The output of layer 1, \vec{a}^1 , is a column vector with Q components equal to zero, except the component with the index of the winning neuron, whose value is set to one. In the second layer, the output is computed as:

$$\vec{a}^2 = \mathbf{W}^L \vec{a}^1 \quad (8)$$

which is a vector that represents a negative or infected air sac, as defined in equation 6. At this point, the learning process takes place by comparing the output in equation 8 with the actual lesion vector in equation 6. If the input vector is classified correctly, then the weight of the winning neuron is moved toward the input vector using the Kohonen rule (Hagan et al., 1996). Conversely, if the input vector is not classified correctly, then the weight vector is moved away from the input vector using the same learning rule. The process is repeated for all vectors \vec{p} in the training set, and the classification weight matrix is modified in each pass. The entire process starts again with the most recent competitive weight matrix until a predetermined number of iterations to fine-tune the competition. A detailed description of the LVQ algorithm can be found in Hagan et al. (1996).

CLASSIFICATION ERROR

The classification error is defined as the fraction of the samples that are misclassified in a given set of samples (Duda and Hart, 1973). In this work, upper and lower error bounds were calculated by considering the holdout error (H) and the resubstitution error (R), respectively (Fukunaga, 1990). In the holdout method, the error is calculated by presenting to the LVQ classifier a training set and simulating the network with an independent test set. In the resubstitution method, the training and test sets are the same. The overall error is considered here as the average of R and H errors.

RESULTS AND DISCUSSION

The knowledge base set and the results of the classifications are shown in figure 5. The lines H and R indicate the

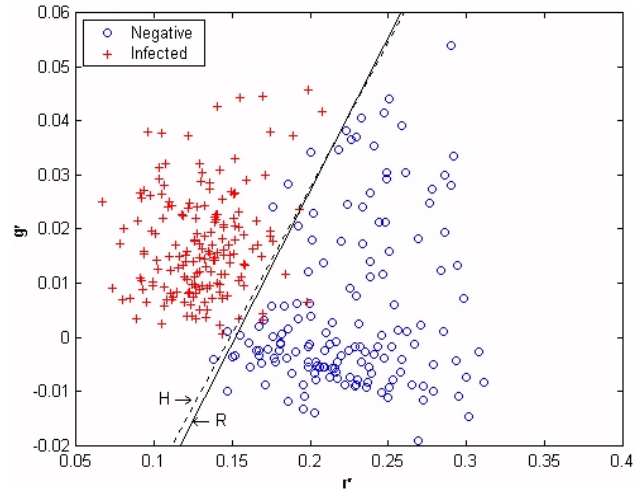


Figure 5. LVQ classification results in the $r'g'$ space. Plus signs indicate infected points, and circles represent negative observations. Lines R and H represent the border decision for upper and low error. An overall accuracy of 96.7% was achieved in the classification.

decision boundaries for holdout and resubstitution methods, as detailed below.

For the holdout method, the knowledge base set was divided, taking odd rows for the training set and even rows for the test set. The distribution of lesions in the training set was 73 negative and 88 infected, while the distribution in the test set was 77 negative and 84 infected. The training set was presented to a LVQ neural network with a learning rate of 0.5 and 150 iterations. The holdout error obtained was $H = 3.8$. The final winning neurons with coordinates (r'_1, g'_1) and (r'_2, g'_2) are the representative points for each lesion category, and a decision borderline can be drawn as the line normal and halfway the segment that join the winning neurons. The boundary decision for the holdout error is represented by the dotted line H in figure 5. Note that the line draws a border between the negative lesion region (to the right), and infected air sac region (to the left).

Similarly, the entire knowledge base set was presented to the same network to calculate the resubstitution error (R). A learning rate equal to 1 and 150 epochs were used in this case. The resubstitution error obtained was $R = 2.8$, and the boundary decision is indicated in figure 5 as the solid line R. Therefore, the overall classification error was 3.3. In other words, the network could correctly classify 96.73% of the observations presented.

It can be observed in figure 5 that lines R and H differ slightly. Because these boundary decision lines correspond to the lower and upper classification error, respectively, the region between the lines can be interpreted as a region in the $r'g'$ space where the classification is not certain. Moreover, for the purpose of lesion assessment, the points inside the

boundary decision lines can be classified as suspicious and can be grouped in the infected category.

The simple two-neuron LVQ classification achieved a high classification accuracy of air sac lesions. Other architectures with more neurons were also tested, but they produced poorer classifications. Additionally, for a practical evaluation of the lesion, it is enough to consider only the $r'g'$ coordinates and their relative location with respect to the boundary decision lines. This fact can be very useful in a real-time application.

CONCLUSIONS

A method to classify air sac lesions according to color coordinates was developed. The method used intensity-normalized color components with proper transformation and a modified competitive neural network to achieve a 96.7% classification accuracy of infected and negative tissue. A total of 100 chickens were infected with *E. coli* for air-sacculitis imaging. The procedure used to inoculate the challenge bacteria produced lesions, categorized as mild and severe, in one of the thoracic air sacs, while preserving the other thoracic air sac. In most of the images, infected and negative air sacs could be imaged simultaneously.

An initial knowledge base set was extracted from the images by averaging normalized color components in 30×30 pixel ROIs. The set was classified into negative, mild, or severe, according to the lesion observed. Preliminary statistical analysis indicated no significant difference between mild and severe points, so the knowledge base set was reclassified into infected and negative points. This limitation does not reduce the potential for a real application since even cases considered mild would be rejected in an actual inspection. Further reduction in the knowledge base set was achieved by considering only independent color components. The initial rgb coordinate system was transformed to reduce the color components to only two.

A two-neuron learning vector quantization network classified the final knowledge base set. Resubstitution and holdout errors were calculated, and the resulting border decision lines gave distinctive classification regions. Therefore, in a practical application, any pixel in an air sac image can be identified as infected or negative by the position of its color coordinates relative to the border decision line. That is, a point to the right of the line is classified as negative, and a point to the left of the line is classified as infected.

However, much research is needed for a real-time implementation. First, the experiment does not reproduce the conditions in the poultry processing plant. In an actual inspection, the chicken carcass is not opened by the abdomen, and evisceration is done through a hole practiced in the lower abdomen. An optical system must be designed to obtain color images of the cavity carcass under such conditions. Second, the knowledge base set can also include points from the background and fat regions for improved classification. Third, the color of fat tissue and infected air sacs is basically the same, so the present method cannot discern those cases. Further study of texture or UV illumination could solve this problem.

Finally, the use of color filters can enhance the color differences between the different factors in the problem (negative and infected air sacs, fat pockets, non-relevant

background, etc.). Prospective research includes the introduction of such optical elements.

ACKNOWLEDGEMENTS

The authors gratefully acknowledge the funding support from the USDA Food Safety Consortium and USDA-ARS, as well as Tyson Foods, Inc., especially Dr. Helen Brown, for kindly providing the chickens used in the experiment. We sincerely thank Dr. Kirk Skeels, DVM, for his knowledge and collaboration at the initial stage of the research. We also wish to thank Dr. Zikuan Chen for valuable discussions, and Mr. George Dwyer for the shop support.

REFERENCES

- Chao, K., Y. R. Chen, and B. Park. 1998. Using fuzzy interference systems for assessments of color imaging in poultry viscera. ASAE Paper No. 983021. St. Joseph, Mich.: ASAE.
- Chen, Y. R. 1992. Classifying diseased poultry carcasses by visible and near-infrared reflectance spectroscopy. *Optics in Agric. and Forestry SPIE* 1836: 46-55.
- Chen, Y. R., and D. R. Massie. 1993. Visible/near-IR reflectance and interactance spectroscopy for detection of unwholesome poultry carcasses. *Trans. ASAE* 36(3): 863-869.
- Chen, Y. R., and W. R. Hruschka. 1998. On-line trials of a chicken carcass inspection system using visible/near-infrared reflectance. ASAE Paper No. 98-3047. St. Joseph, Mich.: ASAE.
- Chen, Y. R., R. W. Huffman, B. Park, and M. Nguyen. 1996. Transportable spectrophotometer system for on-line classification of poultry carcasses. *Applied Spectroscopy* 50(7): 199-219.
- Chtioui, Y., S. Panigrahi, and R. Marsh. 1998. Conjugate gradient and approximate Newton methods for an optimal probabilistic neural network for food color classification. *Optical Eng.* 37(11): 3015-3023.
- Duda, R. O., and P. E. Hart. 1973. *Pattern Classification and Scene Analysis*. New York, N.Y.: John Wiley and Sons.
- Ewing, M. 1997. Basic condemnation criteria for broiler carcasses in the plant. In *32nd National Meeting on Poultry Health and Processing*, 21-28. Ocean City, Md. 15-17 October. Georgetown, Delaware: DPI (Delmarva).
- Fukunaga, K. 1990. *Introduction to Statistical Pattern Recognition*. 2nd ed. Boston, Mass.: Academic Press.
- Goldstein, H. 1980. *Classical Mechanics*. 2nd ed. Oxford, U.K.: Academic Press.
- Gonzalez, R. C., and R. E. Woods. 1992. *Digital Image Processing*. Boston, Mass.: Addison-Wesley.
- Hagan, M. T., H. B. Demuth, and M. Beale. 1996. *Neural Network Design*. Boston, Mass.: PWS Publishing.
- Herenda, D. C., and D. A. Franco. 1996. *Poultry Diseases and Meat Hygiene: A Color Atlas*. Ames, Iowa: Iowa State University Press.
- Huff, G. R., W. E. Huff, J. M. Baloy, and N. C. Roth. 1998. The effects of dexamethasone immunosuppression on turkey osteomyelitis complex in on experimental *Escherichia coli* respiratory infection. *Poultry Science* 77(5): 654-661.
- Jain, R., and R. Kasturi. 1995. *Machine Vision*. New York, N.Y.: McGraw-Hill.
- Park, B., Y. R. Chen, M. Nguyen, and H. Hwang. 1996. Characterizing multispectral images of tumorous, bruised, skin-torn, and wholesome poultry carcasses. *Trans. ASAE* 39(5): 1933-1941.
- Park, B., Y. R. Chen, and M. Nguyen. 1998. Multi-spectral image analysis using neural network algorithm for the inspection of poultry carcasses. *J. Agric. Eng. Research* 69: 351-363.

- Précetti, C. J., and G. W. Krutz. 1993. Building a color classifier. ASAE Paper No. 933003. St. Joseph, Mich.: ASAE.
- Tao, Y., J. Shao, J. K. Skeeles, and Y. R. Chen. 1998a. Spleen enlargement detection of eviscerated turkey by computer vision. In *Proc. Industrial and Environmental Monitors and Biosensors* SPIE 3544: 138–145. Bellingham, Wash.: SPIE.
- Tao, Y., J. Shao, and Y. R. Chen. 1998b. Optical imaging method for internal disease inspection of eviscerated chicken carcasses. ASAE Paper No. 983017. St. Joseph, Mich.: ASAE.
- Tao, Y., J. Shao, J. K. Skeeles, and Y. R. Chen. 2000. Detection of splenomegaly in poultry carcasses by near-UV and color imaging. *Trans. ASAE* 43(2): 469–474.
- USDA–FSIS. 1985. Meat and Poultry Inspection. Committee on the Scientific Basis of the Nation's Meat and Poultry Inspection Program. Washington, D.C.: National Academy Press.

